# Pull-off bond strength of novel wide rounded ends fiber and impact of fiber stretching on fiber/matrix frictional-slip bond strength

## Amjad Khabaz

Check for updates

# Pull-off bond strength of novel wide rounded ends fiber and impact of fiber stretching on fiber/matrix frictional-slip bond strength

Amjad Khabaz (ID)

Civil Engineering Department, Faculty of Engineering, Hasan Kalyoncu University, Gaziantep, Turkey

**ABSTRACT**

This paper presents a study about fiber slippage behavior under direct pull-out and assessment of fiber/matrix pull-off bond strength. This study was prepared through theoretical calculations validated by experimental tests. Theoretically, the study shows a general solution for the fiber-slip mechanism in a general matrix using a new frictional-shear-lag model and an analytical model for pull-off bond strength. Experimentally, pull-out tests were conducted for selected types of single fiber in micro-level (glass, carbon, and short-steel fiber); and macro-level (straight steel fiber). The results showed significant improvements in the pull-off bond strength using novel shape of fiber with wide rounded ends-WESF. The pull-off bond strength in normal-weight concrete was found lower than in lightweight concrete, and the matrix with higher compressive strength improves the pull-off bond strength. Also, the steel fiber showed higher pull-off bond strength compared to glass and carbon fiber; whereas the efficiency of short-steel fiber was higher than the long one. All types of fiber showed that the higher aspect ratio reduces the pull-off bond strength. Using the novel-WESF, the performance of fiber-slip improved 52.65% in normal-weight concrete. Moreover, the fiber-slip performance improved 61.79% in sand-lightweight concrete, and 70.20% in all other types of light-weight concrete.
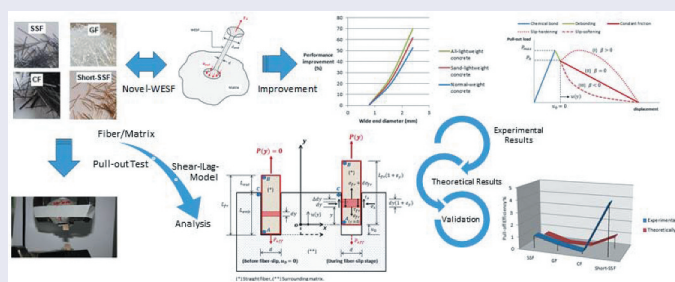
## 1. Introduction

Brittle cement-based composites, including concrete, can be strengthening with fibers as a reinforcement material which improves its toughness, strength and ductility [1]. Fiber bridging strength must be adequate and greater than the initial cracking strength of the matrix. Increasing the fiber bridging strength can be achieved by improving the bond strength of fiber bond to the surrounding cement-based matrix [2]. Fibers also can be used for flexural strengthening of existing beams, where the fiber is usually applied in different forms such as external sheets or bars at the critical shear and bending moment's locations [3]. Furthermore, adding fibers to fresh concrete mix improves the performance of hardened concrete beams and enhances its mechanical behavior against crack-propagation and torsion as well [4–6].

The behavior of reinforced concrete structures subjected to dynamic loads is usually affected by physical factors such as dynamic coefficient of elasticity (modulus of elasticity), absorption of vibration energy, damping coefficient, fatigue strength [7]. According to literature, there are a lot of techniques for evaluation of cracking, fracture and strength in cementitious composites under static, dynamic and fatigue loads besides pull out and pull off tests. There are also many new other nanomaterials used to improve resistance to cracking of construction materials besides fibers, e.g., C-S-H nanoseeds [8]. Furthermore, the type of matrix, as an organic or inorganic, should be considered as an important parameter to control the strength of debonding between the fiber and the matrix, where the strengthening of masonry structures is nowadays performed by means of high-strength fibers embedded in inorganic matrix, such as fiber reinforced concrete matrix, where lime or cement-based matrix is used instead of epoxy adhesive to reduce debonding issues between substrate and matrix, as discussed in [9].

To analyze the mutual slip-movement at the interface between the fiber and the surrounding matrix, a frictional-shear-lag model would be helpful. In the literature, shear-lag models are usually used to analysis the fully bonded case of fiber/matrix system such as: the first shear-lag model developed by Cox [10]; and the shear-lag model developed by Khabaz [11], where the interfacial shear stresses can be found before the fiber slippage occurrence, as discussed by Landis and McMeeking [12]; and Curtin [13]. While these shear-lag models are not suitable to deal with the frictional-sliding stage and the current models in the literature deal with only particular cases of fiber-slip stage, a new frictional-shear-lag model is still required to analyze the frictional fiber-slip mechanism in general case.

The pull-out problem of fibers from different types of surrounding matrix has received considerable attention during the last years, and several worthy contributions have been made as discussed by Lawrence [14]; Freund [15]; and Fuller et al. [16] Shah and Ouyang have prepared an excellent analysis of the pull-out test as presented in [17]. Further light on the fiber-slip at the interface has been shed by investigations including relative slip of rough crack surface as discussed by [18–20].

According to the literature, most models of fiber to matrix interface consider the shear stress at the interface as a function of the fiber-slip displacement [21]. Also, many previous studies simplified the complex three-dimensional behavior at the interface as one-dimensional case [22]. In the solution of one-dimensional case, if the pressure of the surrounding matrix is known, it can be taken into account. Otherwise, a more general

solution is required to take into account the stretching at the interface and the normal relative displacement across the interfacial crack [23].

Recently, some researchers conducted valuable investigations to determine the interfacial shear stresses for specific types of fibers, by using pull out load-displacement models such as: Gopalaratnam and Shah's model for steel fibers [24], and Khabaz's model for steel fibers and glass fibers [25,26]; Wang, Li and Backer's model [27] for nylon, polypropylene and steel fibers; and Redons et al. for PVA fibers [28].

The literature contains huge experimental data and results about the interfacial bonding performance of fiber to matrix [29–36]. These experimental studies have been conducted by using different types and shapes of fiber and matrix, that is, straight (steel, glass, carbon) fibers, fibers with hooked ends, fibers with corrugated shape [37–41]; cementitious and concrete composites, steel-polypropylene hybrid fiber reinforced cementitious composite, etc [11,42–44]. The results showed that the addition of hybrid fibers in the matrix contributes significantly to increasing the maximum and residual pull-out load as well as improving the pull-out energy dissipation capacity. Also, the results showed that for the straight steel fiber, the improving effect of hybrid fiber on the chemical bond is more pronounced than that on the sliding frictional bond [45].

An analytical model for the pullout behavior of single fibers embedded in a concrete matrix for various configurations of fiber type, matrix strength, and embedment condition was proposed by Zhan [46]. In this model, the bond stress-slip relation $\tau(s)$ proposed as in equation (1):

$$\tau(s) = \tau_0 + (\tau_{max} - \tau_0)\exp\left[(s_1 - s)/s_{ref}\right] \tag{1}$$

Where, $(\tau)$ is the interfacial shear stress, $(s)$ is the relative slip defined as the displacement at a point on the fiber axis with respect to the matrix boundary, $(\tau_{max})$ is the bonding strength of the interface, $(\tau_0)$ is the asymptotic value of the frictional stress which stands for the limit value of the bonded interface (such as steel fiber to concrete matrix slippage system), $(s_1)$ is the slip at the fully debonding state, $(s_{ref})$ denotes the parameter controlling the descending branch of the curve.

In the same study, the free-end load-displacement relation ($P$-s) in the pull-out sliding stage can be obtained by considering $(\tau - s)$ relation and solving the equations of force equilibrium and strain compatibility, as in equation (2):

$$P = \pi d\tau(L - s + s_1) \tag{2}$$

In case of constant friction or slip-softening behavior at the interface between the fiber and the matrix (such as straight steel fiber-SSF/concrete-matrix or glass fiber-GF/concrete-matrix), the pullout force ($P$) can be expressed in terms of fiber slip ($u$), using equation (3) as explained in Khabaz's model [25]:

$$P = \tau_s \pi d(l_{emb} - u) \tag{3}$$

Where, $(l_{emb})$ is the embedded length of the fiber in the matrix, $(\tau_s)$ is the frictional bond strength, and $(d)$ is the fiber's diameter. The frictional bond strength $(\tau_s)$ during fiber slippage can be found using equation (4):

$$\tau_s = \frac{P}{\pi d(l_{emb} - u)} \tag{4}$$

The maximum frictional bond strength ($\tau_s = \tau_{smax}$) can be obtained at the onset of fiber slippage, when ($u = 0$ and $P = P_{debond}$).

Furthermore, the surrounding matrix pressure ($\sigma_x$) on the fiber surface, in case of SSF/concrete-matrix, can be predicted experimentally using equation (5), as explained in [23]:

$$\sigma_x = \frac{P_0}{\pi D_f L_{df} Fri_{(f.c)}} \tag{5}$$

Where, ($D_f, L_{df}$) are the diameter and embedded length of the fiber in the matrix, respectively; ($Fri_{(f.c)}$) is the friction coefficient between the fiber and the matrix at the interface, and ($P_0$) is the pull-out load at the full debonding point.

Depending on the accompanying pressure of surrounding concrete ($\sigma_x$), the frictional-bond strength of fiber/matrix can be estimated for different values of friction coefficient $Fri_{(f.c)}$ and different values of fiber embedment length ($L_{df}$) as shown in Figure 1. According to this figure, and whatever the value of SSF embedment length $L_{df}$, it can be noticed that the efficiency of frictional-bond strength was increased 50% in case of increasing the friction coefficient $Fri_{(f.c)}$ from 0.05 to 0.10 (what means increasing the friction coefficient by 100%), and the efficiency of frictional-bond strength was increased 66.7% in case of increasing the friction coefficient $Fri_{(f.c)}$ from 0.05 to 0.15 (what means increasing the friction coefficient by 200%). Therefore, it can be concluded that the friction coefficient $Fri_{(f.c)}$ effects significantly on the efficiency of the frictional-bond strength.

As per in the literature, most researchers were dealing with the pull-out problem as one-dimensional case. Consequently, most previous models of fiber to matrix sliding stage consider the shear stress at the interface as a function of the fiber-slip displacement. While, to make the solution more precise and closer to the actual behavior, more parameters should be taken into account.
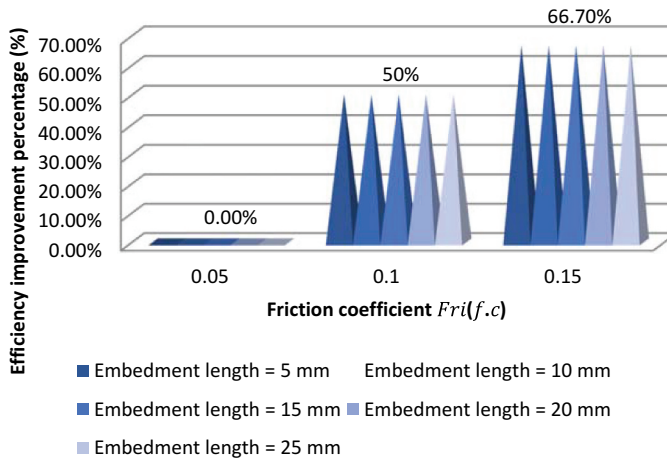


Figure 1. Effect of the friction coefficient of SSF/concrete-matrix on the efficiency of frictional-bond strength.

Furthermore, some missing parameters in previous fiber-slip analytical models can be summarized in these points:

- The effect of the chemical bond of fiber end anchorage (pull-off bond) on the fiber-slip behavior at the interface of fiber/matrix, which will appear directly after full debonding point and before the starting point of fiber sliding.
- Effect of fiber stretching at the interface of fiber/matrix during fiber sliding movement, where most studies neglect this stretching without clear interpretation.
- According to shear stress-relative displacement law, most previous models are suitable to deal with the sliding behavior cases (constant friction, slip-hardening, and slip-softening) at the interface separately. Therefore, developing a new model that considers all these three cases together is still required.
- Effect of the friction coefficient at the interface of fiber/matrix. Where, this coefficient reflects the properties of surface morphology/topology at the interface on the sliding behavior.
- Effect of the accompanying pressure of the surrounding matrix on the frictional sliding behavior.

However, upon further reading, there appears to be a weakness in the recent proposed models of analysis that is the frictional stress as the main parameter of the system was not considered, which is important in the study to reflect the effect of the surface morphology/topology of the fiber and the matrix. The frictional stress and modes are dominated by these parameters. Thus, most previous models studied the fiber-slip mechanism as specific to the fiber type used, but not the universal model. It therefore cannot be considered a fundamental understanding of the general system.

The main objectives of this study are:s

(1) To define the effective parameters such as: pull-off bond strength, the pressure of the surrounding matrix, the stretching at the interface, and the normal relative displacement across the interfacial crack.
(2) To determine the effect of each parameter on the fiber-slip mechanism.
(3) To find a general solution including all considerable parameters.

In this study, a new shear-lag model will be developed for the sliding stage at the interface of the fiber/matrix system. Where, the main effective parameters will be considered in this proposed model, and a general solution of the fiber-slip problem will be introduced. The results of this general solution will be verified through some numerical examples, and a validation will be conducted through experimental records.

## 2. Materials and methods

### 2.1. Fiber-slip categories

The fiber pullout test is often conducted to determine fundamental fiber/matrix interfacial properties, that is, slip-hardening coefficient ($\beta$), frictional bond strength ($\tau_0$), and chemical debonding energy (Gd). In turn, this allows us to determine the fundamental fiber-bridging

relation σ (δ) of the composite (by averaging the contribution from fibers with different embedment length and orientation across the crack plane), which govern the tensile properties of the fiber-reinforced composite [47,48]. As such, the determination of σ (δ) has been resolved in the literature, while including the impact of a fiber/matrix coefficient of friction is still required as proposed by the author of this study in [25]. In fact, the use of the slip-hardening coefficient (β) is implemented in the literature as the fiber slippage regime is often not a constant friction phenomenon, given that there is fiber and/or matrix damage during the slippage regime (depending on the hardness of the fiber relative to the matrix).

Fiber pull out behavior during sliding phase could be grouped into three categories namely:

(a) Constant friction, where the slip-hardening coefficient ($\beta = 0$). In this case, the pull-out load-slip relation is linear, and the shape of the fiber-slip energy zone is triangle, as shown in Figure 2.
(b) Slip-softening, where the slip-hardening coefficient ($\beta < 0$). In this case, the pull-out load-slip relation is nonlinear, and the area of the fiber-slip energy zone is smaller compared to the constant friction behavior, as shown in Figure 3.
(c) Slip-hardening, where the slip-hardening coefficient ($\beta > 0$). In this case, the pull-out load-slip relation is nonlinear as well, but the area of the fiber-slip energy zone is larger compared to the constant friction behavior, as shown in Figure 4.

Where, the fiber slippage movement starts at the point of full debonding with load ($P_0$) and fiber displacement ($S_0$). In Figures 2–4, it has to be known that the first part of the displacement (from 0 to $S_0$) is very small ($S_0 = 0.30 - 0.99mm$) compared to the second part (from $S_0$ to total pull-out).

As shown in Figures 2, 3, 4 the hatched area under the curve of pull-out load-fiber displacement, represents the energy absorption capacity (G) of fiber/matrix regime
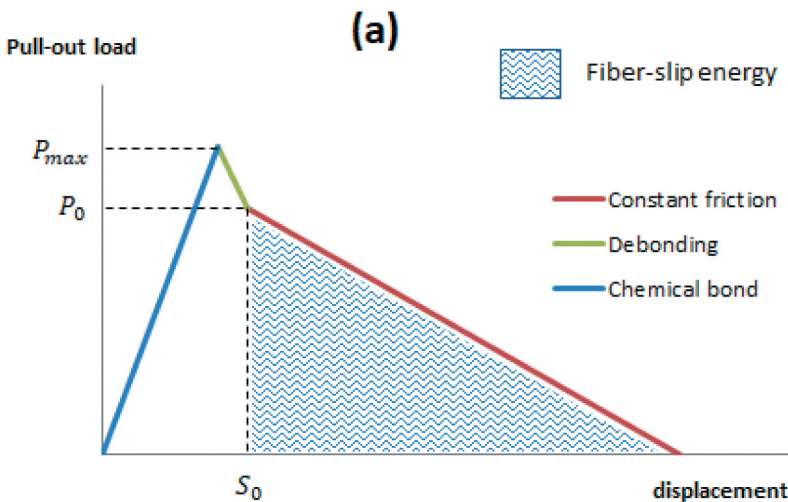


Figure 2. Schematic of single-fiber/matrix slippage regime with constant friction.
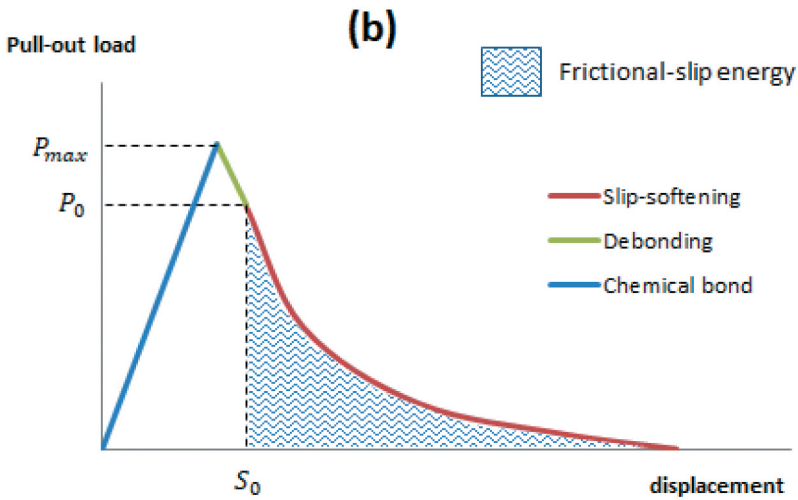
**Figure 3.** Schematic of slip-softening behavior at the interface of single-fiber/matrix slippage regime, where the friction is not constant.
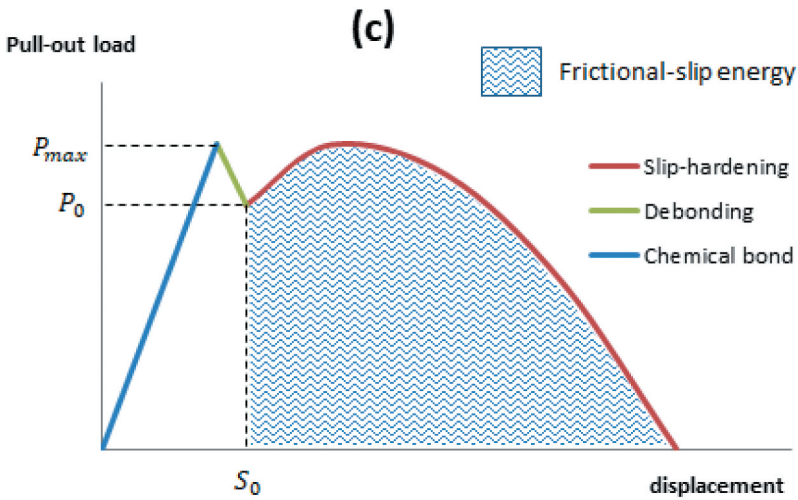


**Figure 4.** Schematic of slip-hardening behavior at the interface of single-fiber/matrix slippage regime, where the friction is not constant as well.

during the frictional sliding stage. The energy absorption capacity can be calculated by equation (6):

$$G = \int_{S_0}^{l_{emb}} P(S)dS \qquad (6)$$

Where, $P(S)$ is the pull-out load during sliding stage, $dS$ is the relative fiber-slip displacement, and $l_{emb}$ is the embedment length of the fiber in the matrix. The energy absorption capability of a composite is attributed to two basic mechanisms:s

(1) material deformation (which occurs first), and
(2) the formation of new surfaces by cracking (which occurs second).

If the supplied energy is enough, a crack may initiate and propagate, thus actuating the second energy-absorbing mechanism. In case of brittle materials, such as cementitious and ceramic matrices, low energy absorption or toughness is shown as a result of the small amount of deformation they can sustain, and their poor resistance to cracking. Thus the total energy absorption capability of fiber/matrix regime can be enhanced either by increasing the path of the cracks during separation or by increasing the fiber's capability to deform. Fibers bridging a crack can absorb energy by deforming and/or pulling out, depending on their bond characteristics. Moreover, the fiber deformation and compliance during pull-out contributes directly to the total deformation of the composite. Thus, the fiber-slip regime, during the frictional sliding stage, can be classified into three categories according to the pull-out process and the energy absorbing mechanisms it generates as mentioned before in this section. Where, slip-hardening happens often with polymer fibers. This happens because the hardness of polymer fibers is usually less than the hardness of the surrounding matrix. Therefore, this type of fibers is damaged and a jamming effect can take place inside the matrix. This leads to an increasing load resisting fiber pullout as shown in Figure 4. This phenomenon is very beneficial as long as the fiber tensile strength is not exceeded. While, constant friction sliding behavior as shown in Figure 2 or slip-softening sliding behavior as shown in Figure 3 are often observed when the fiber hardness is higher than that of the surrounding matrix such as steel-fiber or glass-fiber.

## 2.2. Effect of fiber end anchorage and pull-off bond strength

When the fiber end slips, the effect of fiber end anchorage ($F_1 = P_{off}$) is usually very small, which will be proved in this study, and it can be estimated from the experimental pull-out load versus crack separation curves in addition to fiber/matrix pull-off adhesive bond strength test. Whereas, ($P_{off} = 0$) before complete debonding, see Figure 5. However, despite that the values of pull-off bond strength of traditional straight fibers are expected to be negligible, this study will show specific calculations for this pull-off bond strength. The importance of such calculations is to give a solution key of how the role of pull-off bond strength can be increased to improve the whole system of fiber/matrix against pull-out loads.

Figure 5(a) shows the pull-off test method for in-place tensile bond strength between the fiber end anchorage and concrete surface as an assumed matrix. This method is usually used to conduct the pull-off test according to ASTM C1583. Since the failure of fiber/matrix system will happen because of a pull-off force ($F_1$), and this force should be greater than the tensile bond strength between the fiber end anchorage and the concrete surface; and since the concrete is assumed the weakest material under tension compared to the tensile strength of fiber's material, the pull-off bond strength ($\sigma_P$) can be assumed equals to the matrix direct tensile strength. In case of concrete, the tensile strength is usually estimated at about 10% of its compressive strength ($f_c'$). Therefore, the pull-off force ($F_1$) can be predicted theoretically according to equation (7) as follows:
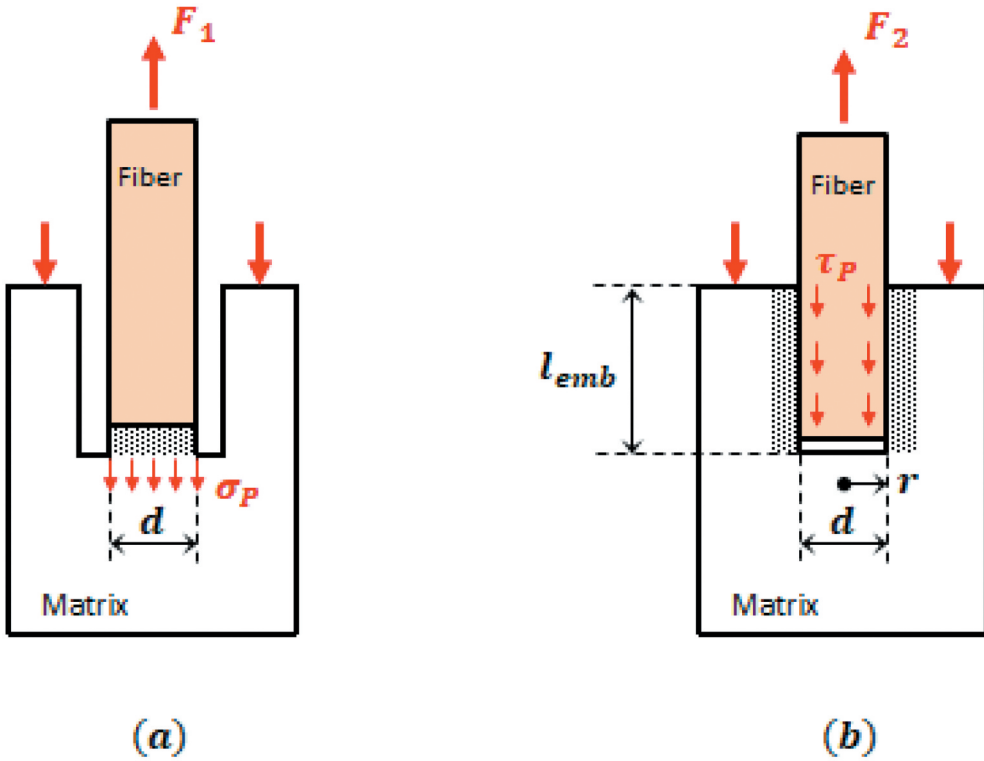
Adhesive matrix layer between the fiber and matrix.

**Figure 5.** Types of fiber/matrix adhesive-bond test: (a) pull-off bond strength; (b) frictional-slip bond strength.

$$F_1 = \sigma_P \left( \frac{\pi d^2}{4} \right) \tag{7}$$

Where, $(\sigma_P)$ is pull-off fiber/matrix bond strength, and $(d)$ is the fiber diameter.

Figure 5(b) shows a model of fiber/matrix slippage system. According to this model, when the fiber/matrix system is fully deboned, the pull-out force $(P_0)$ can be considered as the applied tensile force $(F_2 = P_0)$, where the chemical bond strength is fully failed. Since the value of the interfacial shear stress is usually small during fiber-slip stage, and to simplify the calculations, the fiber-stretch will be neglected, and then the interfacial shear stress can be assumed as uniform; consequently, the maximum interfacial shear stress $(\tau_P)$ can be calculated by dividing the applied pull-out force $(F_2)$ with the embedded surface of the fiber in the matrix $(2\pi r l_{emb})$, as expressed in equation (8):

$$\tau_P = \frac{F_2}{2\pi r l_{emb}} \tag{8}$$

Where, $(F_2)$ is the applied pull-out force at the full-debonding point $(F_2 = P_0)$, and $(r)$ is the fiber radius $(d = 2r)$.

Since the fiber slippage starts directly when the fiber displacement exceeds the full-debonding point, the interfacial shear stress ($\tau_P$) can be assumed as the flexural strength of the matrix or the modulus of rupture ($f_r$). In case of concrete, the ACI Code prescribes the modulus of rupture ($f_r$) in terms of concrete compressive strength () as in equation (9):

$$f_r = 0.62\lambda\sqrt{f'_c}\left(\frac{N}{mm^2}\right) \tag{9}$$

Where, $\lambda$ is a modification factor for the type of concrete as follows:
$\lambda = 1.0$ Normal-weight concrete
$\lambda = 0.85$ Sand-lightweight concrete
$\lambda = 0.75$ For all-lightweight concrete

## 2.3. Experimental program

The aim of this experimental program is to evaluate the frictional-slip bond characteristics of different types of fibers in concrete matrix, as an inorganic matrix, using ordinary cement mortar. Furthermore, the effect of fiber and matrix properties on pull-out behavior will be examined. The tensile test load of pull-out machine is up to 100 KN. The test load was modernized for a small force range suitable for a single glass and carbon fiber. This machine can be operated with a standard commercial PC or laptop. Test speeds of this machine are available from 0.0005 to 1500 mm/min. The maximum crosshead return speed of the used machine is 2000 mm/min; the maximum deviation from the set drive speed is 0.05% of the actual velocity, and the drive travel resolution is 0.0348 µm. The pull-out displacements of fiber during the tests were monitored and recorded by a camera with a vertical image resolution equals 1536 px.

Two categories of pull-out tests were conducted for single fiber embedded into concrete matrix as follows:

(a) Using embedment length of fiber equal to 50% from its total length.
(b) Using different ratios of embedment length ranges from 7.5% to 50% from the total length of fiber.

Also, four types of fiber were used:

- Straight steel fiber-SSF
- Glass fiber-GF
- Carbon fiber-CF
- Short-SSF

The main physical and mechanical properties of these fibers are shown in Table 1.

The matrix in this experimental program was prepared from normal weight concrete using ordinary cement mortar in addition to some chemical additives to improve the workability situation of the mixture. Three concrete mixtures were prepared using a laboratory trial method, M1 for the surrounding matrix of SSF and Short-SSF, M2

**Table 1.** Physical and mechanical properties of fibers.

| Fiber type | Length (mm) | Diameter (μm) | Aspect ratio (L/r) | Density (Kg/m$^3$) | Tensile strength (MPa) | Young's Modulus (GPa) | Poisson's ratio | Strain capacity (%) |
|---|---|---|---|---|---|---|---|---|
| SSF | 50 | 800 | 125 | 7850 | 1200 | 200 | 0.28 | 2.3 |
| GF | 40 | 15 | 5333 | 1850 | 1500 | 70 | 0.20 | 2 |
| CF | 50 | 7.5 | 13,333 | 1750 | 1970 | 240 | 0.26 | 0.8 |
| Short-SSF | 6 | 160 | 75 | 7850 | 1200 | 200 | 0.28 | 2.3 |

for GF, and M3 for CF. The cement amount was designed to obtain sufficient full-bond strength between all concrete mix components, and the content of water was calculated to conduct a well hydration process for the cement paste, and to obtain an acceptable workability, where the ratio of water to cement (w/c) was 44.4% in M1, 37% in M2, and 424% in M3. Three types of sand aggregates were used; its sizes were ranged from 0 to 0.5 mm, from 0.3 to 2.5 mm and from 2 to 4 mm, with quantities suitable for each type of fiber to obtain an acceptable morphology/topology surface of fiber/matrix, in addition to filler (dolomite powder) and microsilica, which are necessary to obtain an acceptable smoothness in the curve of graded aggregates. To improve the workability of fresh concrete and to reduce the air contents, and also to adjust the voids between the concrete particles after hardening; two types of chemical additives were used, SIKA EVO 26 and SIKA AER S. After mixing, where the concrete mixes were homogeneous with an acceptable workability; the settlement of the fresh concrete according to slump test between around 7 cm. The density of fresh concrete was 2196 kg/m$^3$ for M1, 1955.3 kg/m$^3$ for M2, and 2004.71 kg/m$^3$ for M3 (see Table 2). The Young's modulus of hardened concrete after 28 days was about 30,000 MPa, and the compressive strength of all mixes was around 21 MPa. Poisson's ratio was defined as 0.20 for all mixes as well.

Six groups of single fiber embedded into concrete matrix were prepared for pull-out test, and each group consists of various samples as the following:

In the first group, 3 samples were prepared using Straight Steel Fiber-SSF with embedded length equal to (0.5 L = 25 mm), where (L = 50 mm) is the total length of SSF.

In the second group, 3 samples were prepared using Glass Fiber-GF with embedded length equal to (0.5 L = 20 mm), where (L = 40 mm) is the total length of GF.

In the third group, 3 samples were prepared using Carbon Fiber-CF with embedded length equal to (0.5 L = 25 mm), where (L = 50 mm) is the total length of CF.

**Table 2.** Proportions of concrete mixtures.

| Concrete mix proportion | Portion vol.=1m$^3$ | | |
|---|---|---|---|
| | M1 | M2 | M3 |
| Cement II 42.5 A-V (kg) | 556 | 575 | 615 |
| Water (liter) | 247 | 213 | 261 |
| Microsilica (kg) | 81 | 49 | 54 |
| Dolomite powder filler (kg) | 150 | 182 | 154 |
| Sand 0–0.5 mm (kg) | 288 | 427 | 283 |
| Sand 0.3–2.5 mm (kg) | 620 | 370 | 277 |
| Sand 2–4 mm (kg) | 243 | 129 | 349 |
| Admixture SIKA EVO 26 (liter) | 9 | 8.7 | 9.91 |
| Admixture SIKA AER S (10%) (liter) | 2 | 1.6 | 1.8 |
| Density (kg/m$^3$) | 2196 | 1955.3 | 2004.71 |

In the fourth group, 3 samples were prepared using Short-SSF with embedded length equal to (0.5 L = 3 mm), where (L = 6 mm) is the total length of Short-SSF.

In the fifth group, 5 samples were prepared using SSF with embedded length equal to (5 mm, 10 mm, 15 mm, 20 mm, and 25 mm).

In the sixth group, 4 samples were prepared using GF with embedded length equal to (3 mm, 5 mm, 10 mm, and 20 mm).

All samples were cured by the moist-curing method, with room temperature 25 − 30, and humidity ranges from 40% to 80%, where after casting a nylon cover was put over samples, in this case the moisture of concrete will evaporate slowly and stronger concrete can be obtained, see Figure 6.

After 28 days, a pull-out test was conducted for each sample. The pull out speed was maintained at 1 mm/min for SSF and 0.1 mm/min for GF, CF, and Short-SSF. Then records of force-displacement were taken to observe the mechanical behavior of fiber inside the concrete compared to the increment of pull-out tensile forces. Using these records, curves of force-displacement can be drawn, then bonding and debonding points can be found for each sample, where these two points are important to validate the theoretical analysis of pull-off bond strength capacity; and frictional-interfacial stage can be shown as well, which is important to validate the analytical shear-lag-model of this study in addition to the derived governing equations.

## 2.4. Frictional-Shear-Lag model and governing equations

As mentioned before in the introduction section of this study, to analyze the mutual slip-movement at the interface between the fiber and the surrounding matrix, a frictional-shear-lag model would be helpful. Figure 7 shows a new shear-lag model proposed by the
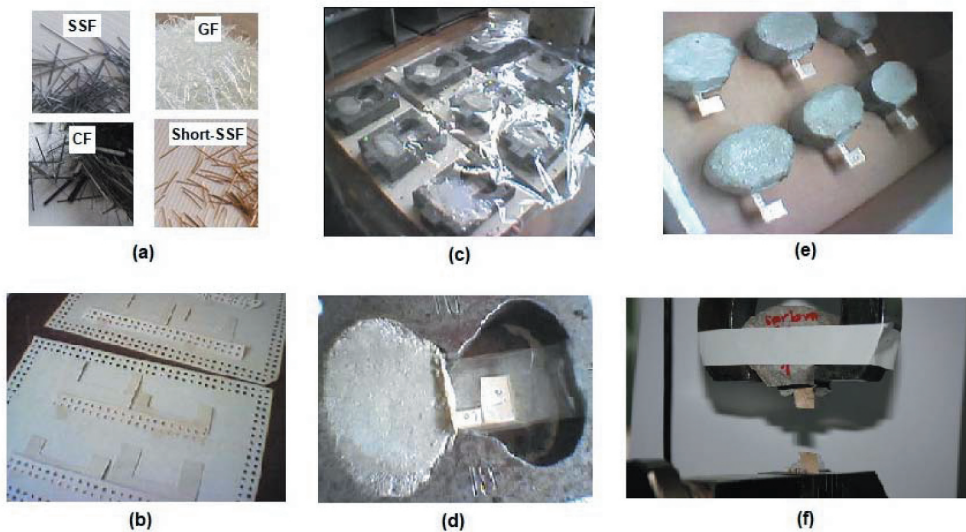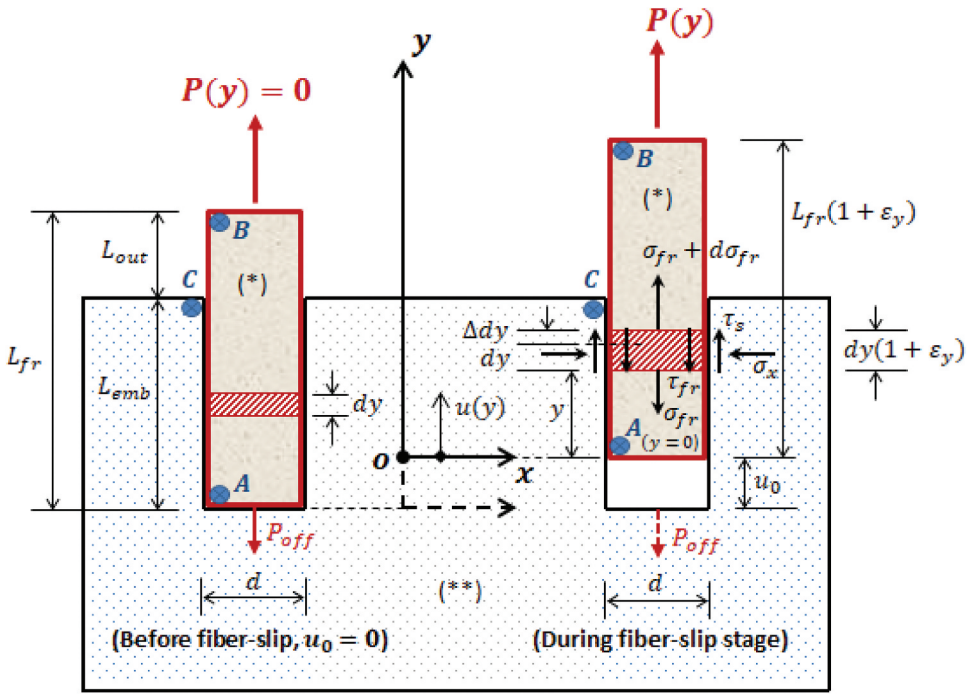


**Figure 6.** Experimental procedure of pull-out test: (a) types of used f fiber; (b) carton chairs for microfiber protection; (c) casting and curing of samples; (d) plastic chairs to satisfy fiber level; (e) releasing samples from moulds; (f) pull-out test.

**Figure 7.** Frictional-Shear-Lag model of single fiber slippage in a matrix under direct pull-out load.

author of this paper. Where the fiber/matrix system is prepared for theoretical analysis in two cases:

(1) Before fiber-slip, where the fiber-slip at point (A) assumed to be zero ($u_0 = 0$), in this case the fiber is not loaded in ($y$) direction, therefore the pull-out force $P(y) = 0$ and the pull-off strength force $P_0 \neq 0$. The point (B) will be used as a reference for observing the fiber movement at the free end of fiber, whereas point (C) will be used as a reference point for the free end of matrix. The original length of fiber between (A) and (B) is ($L_{fr}$), and the embedded length of fiber in the matrix between (A) and (C) is called ($L_{emb}$), while the free part of fiber out of the matrix is called ($L_{out}$). For analysis, a small strip from the fiber with initial length equal to ($dy$) will be studied. The fiber diameter will be called (d) as well. Axis ($x$) is a moveable axis and always located at the bottom of fiber. Axis ($y$) is vertically a moveable axis as well, where the origin ($o$) can move along ($y$) direction.

(2) During fiber-slip stage, the fiber will be loaded by pull-out load $P(y) > 0$. In this case the fiber will slide along ($y$) direction with displacement equal to $u(y)$, and then the pull-off strength will be failed and $P_0 = 0$. The displacement of point (A) will be called ($u_0$), and always ($y = 0$) at point (A). Because of fiber stretching the original length of fiber will be extended between (A) and (B), and the total length of fiber will be $L_{fr}(1 + \varepsilon_y)$, where ($\varepsilon_y$) is the strain of fiber in ($y$) direction. During the frictional-sliding stage, the strip will be under normal stress ($\sigma_{fr}$) at the bottom

level, and $(\sigma_{fr} + d\sigma_{fr})$ at the upper level. Therefore, the strip will be stretched, the stretching will be assumed $(\Delta dy)$, then $(\varepsilon_y = \frac{\Delta dy}{dy})$, and the length of strip after stretching will equal to $dy(1 + \varepsilon_y)$. Due to fiber sliding, the friction at the interface of fiber/matrix will convert the pressure $(\sigma_x)$ of surrounding matrix to a frictional-shear stress $(\tau_s = \tau_{fr})$ on the matrix and the fiber as shown in Figure 7.

The governing equations can be derived by taking the equilibrium in $(y)$ direction of effective stresses on the fiber strip during fiber-slip stage as the following:

$$\sigma_{fr} + d\sigma_{fr} - \sigma_{fr})\frac{\pi d^2}{4} = \pi d\tau_{fr}(dy + \Delta dy) \tag{10}$$

Rearranging the left side without $(\sigma_{fr})$ and multiplying the right side by $(\frac{dy}{dy})$, equation (10) can be written in a new shape as the following:

$$d\sigma_{fr}\frac{\pi d^2}{4} = \pi d\tau_{fr}\left(1 + \frac{\Delta dy}{dy}\right)dy \tag{11}$$

In equation (11), the left side represents the pull-out force which effects on the fiber strip $dP(y)$, and also in the right side $\frac{\Delta dy}{dy}$ represents the strain of fiber strip $(\varepsilon_y)$. Therefore, this equation can be written in a new shape once again as follows:

$$dP(y) = \pi d\tau_{fr}(1 + \varepsilon_y)dy \tag{12}$$

Conducting integration to both sides of equation (12) along the effective embedded length of fiber $(L_{emb} - u_0)$, with respect to $(dy)$ as in equation (13), will lead to an initial shape of pull-out force formula (14) as follows:

$$\int_0^{L_{emb} - u_0} dP(y) = \int_0^{L_{emb} - u_0} \pi d\tau_{fr}(1 + \varepsilon_y)dy \tag{13}$$

$$P(y) = \int_0^{L_{emb} - u_0} \pi d\tau_{fr}(1 + \varepsilon_y)dy \tag{14}$$

The pull-off bond strength $(P_{off})$ can be considered in equation (14) and then the initial shape of pull-out force can be written as the following:

$$P(y) = P_{off} + \int_0^{L_{emb} - u_0} \pi d\tau_{fr}(1 + \varepsilon_y)dy \tag{15}$$

In traditional shape of straight fiber, the value of pull-off bond is usually very small $(P_{off} \cong 0)$, and it can be neglected. Therefore, in the next sections a novel shape of straight steel fiber with wide ends will be introduced under the name (WESF). These wide ends will support and improve the role of pull-off bond strength against pull-out loads by significant ratios.

Assuming the fiber under linear elastic behavior, in $(y)$ direction the fiber strain $(\varepsilon_y)$ in equation (15) can be found according to Hook's law as follows:

$$\sigma_{fr} = \varepsilon_y E_{fr} \tag{16}$$

Where, $(E_{fr})$ represents the elasticity modulus of fiber.

Also, since the value of pull-out load during the fiber slippage stage is small, the strain of fiber in $(x)$ direction will be very small $(\varepsilon_x \cong 0)$. Therefore, the effect of Poisson's ratio (v) can be neglected:

$$v = \frac{\varepsilon_x}{\varepsilon_y} \cong 0 \tag{17}$$

According to this, the fiber cross-sectional area $(A_{fr})$ can be assumed as constant and equal to:

$$A_{fr} = \frac{\pi d^2}{4} \tag{18}$$

On the other hand, the normal stress on the fiber because of pull-out load $(\sigma_{fr})$ can be found as follows:

$$\sigma_{fr} = \frac{P(y)}{A_{fr}} \tag{19}$$

According to the equations (16) and (19), taking into account that the strain of fiber is not constant, but a function of (y), we can write:

$$\varepsilon_y(y)E_{fr} = \frac{P(y)}{A_{fr}} \tag{20}$$

Therefore, the fiber strain formula can be written as follows:

$$\varepsilon_y(y) = \frac{4P(y)}{\pi d^2 E_{fr}} \tag{21}$$

The slippage distance, $u(y)$, of an infinitesimal fiber segment at $(y)$ is equal to the sum of the fiber embedded end slippage distance, $u_0$, plus the elastic elongation of the fiber segment located between $(y = 0)$ and $(y = y)$, and the equation of, $u(y)$, can be written as follows:

$$u(y) = u_0 + \int_0^y \varepsilon_y(y)dy \tag{22}$$

Where, $(y_{max} = L_{fr})$, and the total length of fiber after elastic elongation will be considered as, $L_{fr}(1 + \varepsilon_y)$.

According to equation (22) and (15), it is clear that the shear stress $(\tau_{fr})$ and the interfacial slip of fiber $(u_0)$ are functions of position along the interface, where the fiber slippage is non-uniform as in the case of a fiber bridging across a matrix crack. Therefore, we can write:

$$\tau_{fr} = \tau_{fr}(u_0) \tag{23}$$

Bao and Sang, as discussed in [49], proposed a model to describe a linear relationship between $(\tau_{fr})$ and $u(y)$, as follows:

$$\tau_{fr} = \tau_0\left(1 + \beta\frac{u_0}{d}\right) \tag{24}$$

Where, $(\tau_0)$ is the frictional sliding shear stress at the full-debonding point where the fiber slippage equal to zero $(u_0 = 0)$, and $(\beta)$ is a non-dimensional hardening parameter, and $(d)$ is the fiber diameter.

In the proposed frictional shear-lag model of this study, as shown in Figure 7, the fiber is assumed to be pulled out of the matrix without rupture in a rigid manner, this means that the elastic stretch of the fiber is negligible compared to the fiber end displacement during the pull-out stage. Therefore, we can write:

$$\varepsilon_y = \frac{\Delta dy}{dy} = 0 \tag{25}$$

And then, according to equation (14), the pull-out force, $P(y)$, can be found as follows:

$$P(y) = \int_0^{L_{emb}-u_0} \pi d\tau_{fr} dy \tag{26}$$

$$P(y) = \tau_{fr} \pi d(L_{emb} - u_0) \tag{27}$$

$(\tau_{fr})$ in equation (27) can be replaced by $(\tau_0)$ if $(\beta = 0)$, and this will be a special case of equation (24). Also, in case of constant friction during fiber-slip stage, $(\beta)$ can be considered equal to zero and then $(\tau_{fr} = \tau_0)$ as well.

Substituting $(\tau_{fr})$ in equation (27) by the right side of equation (24) will lead to a new formula for the pull-out load, $P(y)$, in terms of fiber slippage, $u(y)$, as follows:

$$P(y) = \tau_0 \left(1 + \beta \frac{u_0}{d}\right) \pi d(L_{emb} - u_0) \tag{28}$$

Rearranging equation (28) will give:

$$P(y) = \tau_0 \pi d(L_{emb} - u_0) + \tau_0 \beta u_0 \pi (L_{emb} - u_0) \tag{29}$$

Solving the brackets in equation (29) will give:

$$P(y) = \tau_0 \pi d L_{emb} - \tau_0 \pi d u_o + \tau_0 \beta u_0 \pi L_{emb} - \tau_0 \beta \pi (u_0)^2 \tag{30}$$

In equation (30), ignoring the second-order terms in $(u_0)^2$ is suitable because of small values of fiber slippage $(u_0)$, and the pull-out force, $P(y)$, can be expressed in terms of fiber slippage $(u_0)$ as follows:

$$P(y) = \tau_0 \pi d \left[ L_{emb} + u_0 \left( \beta \frac{L_{emb}}{d} - 1 \right) \right] \tag{31}$$

equation (31) represent a general solution of fiber-slip behavior under direct pull-out loading, and according to the value of $(\beta)$ the shape of load-displacement curve in the sliding stage will appear similar to one of these three categories as shown in Figure 8:

   (I) Slip-hardening if $(\beta > 0)$
  (II) Constant friction if $(\beta = 0)$
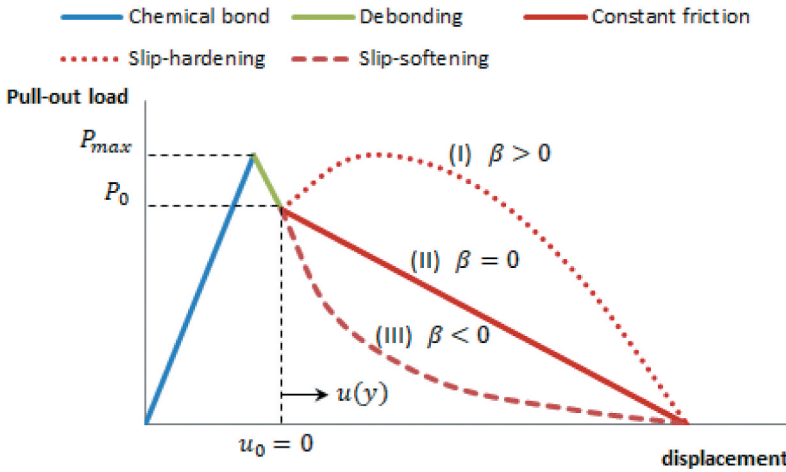 (III) Slip-softening if $(\beta < 0)$

**Figure 8.** Schematic of single fiber load-displacement curve under direct pull-out in general case including three categories of fiber-slip behavior.

Also, in equation (31) the stress ($\tau_0$) can be found from the force-displacement curve of pull-out test using equation (32) as follows:

$$\tau_0 = \frac{P_0}{\pi d L_{emb}}$$ (32)

Where, ($P_0$) is the pull-out load at the full-debonding point, see Figure 8.

In case of slip-softening or constant friction, as a special case, for fibers such as (steel, glass, carbon) where ($\beta = 0$), the pull-out force, $P(y)$, in equation (31) will be written as follows:

$$P(y) = \tau_0 \pi d (L_{emb} - u_0)$$ (33)

Equation (33) shows the same result which was obtained from equation (27) when replacing ($\tau_{fr}$) by ($\tau_0$) in case of ($\beta = 0$).

## 3. Results and Discussion

### 3.1. Assessment of pull-off bond strength capacity and novel-WESF

Depending on the analytical models of pull-off bond strength and frictional-slip bond strength as shown previously in Figure 5 section (2.2) in this study, and using the related equations (7,8,9); the effect of fiber end anchorage bond strength (pull-off) can be evaluated theoretically as shown in Table 3 with respect to different values of matrix compressive strength, different types of concrete matrix (normal weight concrete, sand-light weight concrete, all-light weight concrete), and a specific value of fiber aspect ratio ($L_{fr}/r$) according to the type of fiber.

According to the calculations of Table 3, the results show that the efficiency of pull-off bond strength, in case of normal-weight concrete, is lower than the case of lightweight concretes. While, the higher compressive strength of concrete improves the role of pull-off bond strength, see Figure 9. Also, the role of pull-off bond strength is more effective in

case of steel fiber compared to glass fiber and carbon fiber, see Figure 10. Accordingly, the role of pull-off bond strength in case of glass fiber and carbon fiber can be neglected. Moreover, despite that the results show a higher value of pull-off load capacity in case of long straight steel fiber-SSF compared to the short-SSF, the efficiency of pull-off bond strength in case of short-SSF is higher than the efficiency of pull-off bond strength of the long straight steel fiber-SSF, see Figure 11. Also, in all types of fiber, the results show that the higher aspect ratio of fiber ($L_{fr}/r$) effects negatively on the efficiency of pull-off bond strength, see Figure 12.

Furthermore, in case of straight steel fiber-SSF, the effect of fiber end anchorage bond strength (pull-off) can be evaluated theoretically as shown in Table 4, in particular with reference to values reported in Table 3, and with respect to different types of concrete matrix (normal weight, sand light-weight, and all other types of lightweight concretes) using different values of fiber end anchorage diameter ($d_{end}$). The results show that increasing the diameter of the fiber end anchorage improves the pull-off bond strength and consequently a higher pull-out force will be required to obtain the same fiber-slip

**Table 3.** Theoretical evaluation of the effect of pull-off bond strength compared to the frictional-slip bond strength on the capacity of frictional-slip load of fiber/concrete system.

| Fiber type | λ | $f'_c$ (MPa) | $L_{fr}$ (mm) | $d$ (mm) | $L_{fr}/r$ | $\sigma_P$ (MPa) | $\tau_P$ (MPa) | $F_1$ (N) | $F_2$ (N) | $(F_1/F_2) \times 100$ (%) |
|---|---|---|---|---|---|---|---|---|---|---|
| Straight steel fiber-SSF | 1 | 21 | 50 | 0.8 | 125 | 2.1 | 2.84 | 1.06 | 178.44 | 0.59 |
| | | 35 | | | | 3.5 | 3.67 | 1.76 | 230.59 | 0.76 |
| | | 50 | | | | 5.0 | 4.38 | 2.51 | 275.20 | 0.91 |
| | 0.85 | 21 | | | | 2.1 | 2.42 | 1.06 | 152.05 | 0.70 |
| | | 35 | | | | 3.5 | 3.12 | 1.76 | 196.04 | 0.90 |
| | | 50 | | | | 5.0 | 3.73 | 2.51 | 234.36 | 1.07 |
| | 0.75 | 21 | | | | 2.1 | 2.13 | 1.06 | 133.83 | 0.79 |
| | | 35 | | | | 3.5 | 2.75 | 1.76 | 172.79 | 1.02 |
| | | 50 | | | | 5.0 | 3.29 | 2.51 | 206.72 | 1.21 |
| Glass fiber-GF | 1 | 21 | 40 | 0.015 | 5333 | 2.1 | 2.84 | 0.00037 | 2.68 | 0.014 |
| | | 35 | | | | 3.5 | 3.67 | 0.00062 | 3.46 | 0.018 |
| | | 50 | | | | 5.0 | 4.38 | 0.00084 | 4.13 | 0.020 |
| | 0.85 | 21 | | | | 2.1 | 2.42 | 0.00037 | 2.28 | 0.016 |
| | | 35 | | | | 3.5 | 3.12 | 0.00062 | 2.94 | 0.021 |
| | | 50 | | | | 5.0 | 3.73 | 0.00084 | 3.52 | 0.023 |
| | 0.75 | 21 | | | | 2.1 | 2.13 | 0.00037 | 2.01 | 0.018 |
| | | 35 | | | | 3.5 | 2.75 | 0.00062 | 2.59 | 0.024 |
| | | 50 | | | | 5.0 | 3.29 | 0.00084 | 3.10 | 0.027 |
| Carbon fiber-CF | 1 | 21 | 50 | 0.0075 | 13,333 | 2.1 | 2.84 | 0.000093 | 1.67 | 0.0056 |
| | | 35 | | | | 3.5 | 3.67 | 0.000155 | 2.16 | 0.0072 |
| | | 50 | | | | 5.0 | 4.38 | 0.000221 | 2.58 | 0.0086 |
| | 0.85 | 21 | | | | 2.1 | 2.42 | 0.000093 | 1.43 | 0.0065 |
| | | 35 | | | | 3.5 | 3.12 | 0.000155 | 1.84 | 0.0084 |
| | | 50 | | | | 5.0 | 3.73 | 0.000221 | 2.20 | 0.0100 |
| | 0.75 | 21 | | | | 2.1 | 2.13 | 0.000093 | 1.25 | 0.0074 |
| | | 35 | | | | 3.5 | 2.75 | 0.000155 | 1.62 | 0.0096 |
| | | 50 | | | | 5.0 | 3.29 | 0.000221 | 1.94 | 0.0114 |
| Short-SSF | 1 | 21 | 6 | 0.16 | 75 | 2.1 | 2.84 | 0.042 | 4.28 | 0.98 |
| | | 35 | | | | 3.5 | 3.67 | 0.070 | 5.53 | 1.27 |
| | | 50 | | | | 5.0 | 4.38 | 0.101 | 6.60 | 1.53 |
| | 0.85 | 21 | | | | 2.1 | 2.42 | 0.042 | 3.65 | 1.15 |
| | | 35 | | | | 3.5 | 3.12 | 0.070 | 4.70 | 1.49 |
| | | 50 | | | | 5.0 | 3.73 | 0.101 | 5.62 | 1.80 |
| | 0.75 | 21 | | | | 2.1 | 2.13 | 0.042 | 3.21 | 1.31 |
| | | 35 | | | | 3.5 | 2.75 | 0.070 | 4.14 | 1.69 |
| | | 50 | | | | 5.0 | 3.29 | 0.101 | 4.96 | 2.04 |
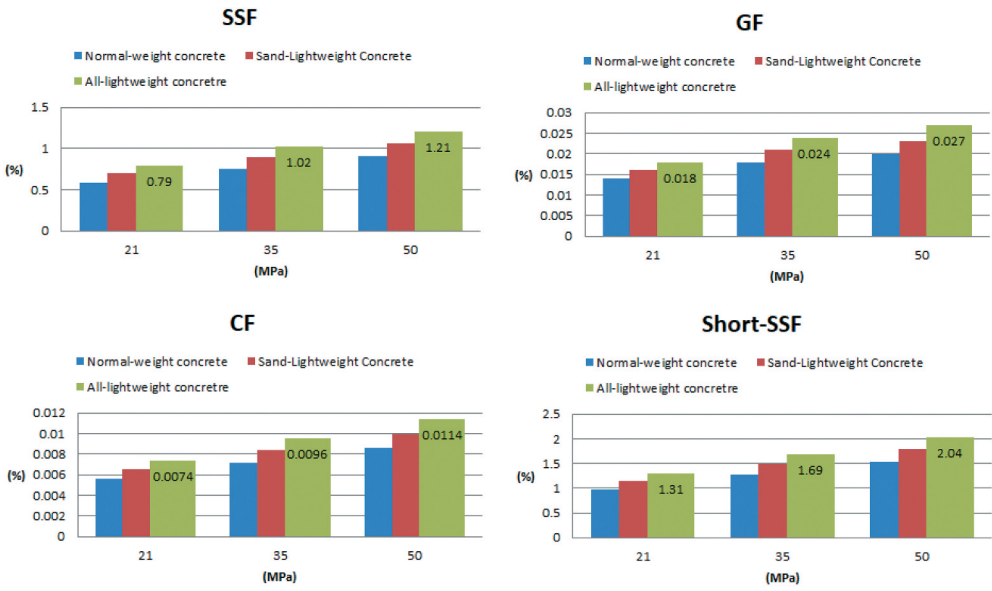
**Figure 9.** Effect of concrete compressive strength (horizontal axis) and concrete type on the efficiency of pull-off bond strength (vertical axis) for different types of fiber.
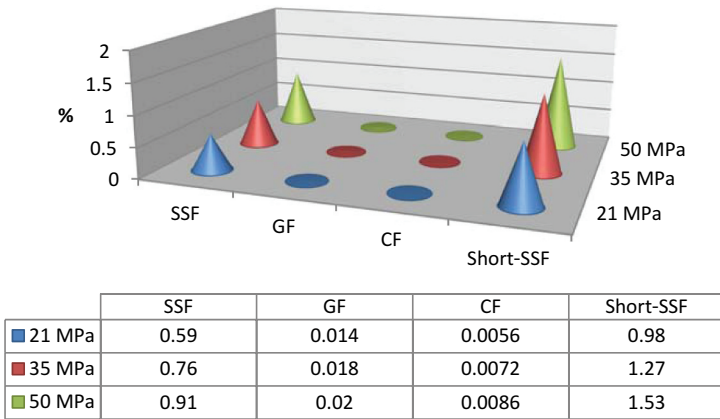


|  | SSF | GF | CF | Short-SSF |
|---|---|---|---|---|
| 21 MPa | 0.59 | 0.014 | 0.0056 | 0.98 |
| 35 MPa | 0.76 | 0.018 | 0.0072 | 1.27 |
| 50 MPa | 0.91 | 0.02 | 0.0086 | 1.53 |

**Figure 10.** Effect of fiber type on the pull-off bond strength efficiency (%) for different types of fiber in case of normal-weight concrete with compressive strength 21, 35, 50 MPa.

displacement. On other hand, decreasing the fiber diameter of its embedment length improves the frictional-slip bond of the fiber as discussed by Khabaz in [25]. Therefore, it can be concluded that the efficiency of fiber/matrix system might be improved, in all types of concrete (normal and lightweight), by decreasing the fiber diameter along its embedment length, and by increasing the cross-sectional area of the fiber at its end anchorage as shown in Figure 13, where this figure shows a recommended shape of wide ends steel fiber-WESF. Also, it can be concluded that the use of steel fiber with wide ends-WESF leads to significant improvements against pull-out resistance in case of lightweight concrete compared to normal weight concrete.
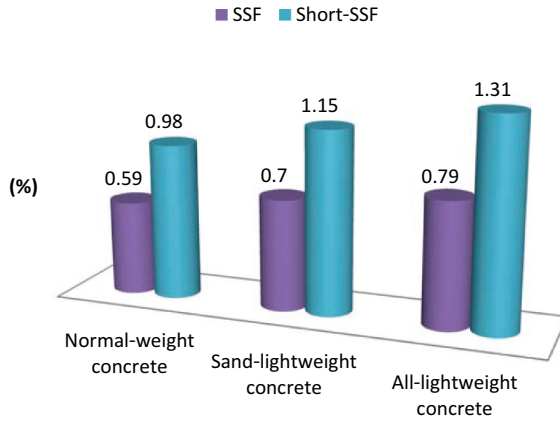
**Figure 11.** Pull-Off bond strength efficiency (%) of Short-SSF compared to SSF using different types of concrete with compressive strength equal to 21 MPa.
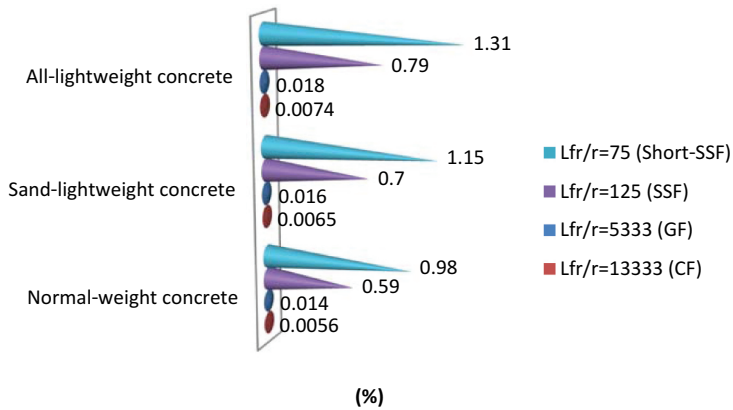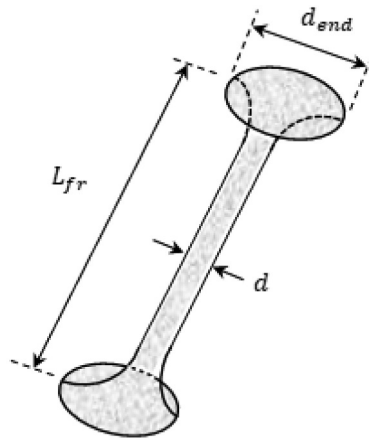


**Figure 12.** Effect of aspect ratio ($L_{fr}/r$) on the pull-off bond strength efficiency (%) using different types of concrete with compressive strength equal to 21 MPa.

**Table 4.** Effect of the cross-sectional area of the fiber end anchorage on the efficiency of pull-off bond strength, and on the capacity of frictional-slip load of fiber/concrete system.

| Fiber type | $\lambda$ | $f'_c$ (MPa) | $L_{fr}$ (mm) | $d$ (mm) | $d_{end}$ (mm) | $\sigma_P$ (MPa) | $\tau_P$ (MPa) | $F_1$ (N) | $F_2$ (N) | $(F_1/F_2) \times 100$ (%) |
|---|---|---|---|---|---|---|---|---|---|---|
| Straight steel fiber-SSF | 1 | 21 | 50 | 0.8 | 0.8 | 2.1 | 2.84 | 1.06 | 178.44 | 0.59 |
| | | | | | 1.6 | | | 4.22 | | 2.36 |
| | | | | | 2.4 | | | 9.50 | | 5.32 |
| | 0.85 | | | | 0.8 | | 2.42 | 1.06 | 152.05 | 0.70 |
| | | | | | 1.6 | | | 4.22 | | 2.78 |
| | | | | | 2.4 | | | 9.50 | | 6.25 |
| | 0.75 | | | | 0.8 | | 2.13 | 1.06 | 133.83 | 0.79 |
| | | | | | 1.6 | | | 4.22 | | 3.15 |
| | | | | | 2.4 | | | 9.50 | | 7.10 |

| Length $L_{fr}$ (mm) | Diameter (µm) | | Aspect ratio $(L_{fr}/r)$ | Density $(Kg/m^3)$ | Tensile strength (MPa) | Young's Modulus (GPa) | Poisson's ratio | Strain capacity (%) |
|---|---|---|---|---|---|---|---|---|
| | $d$ | $d_{end}$ | | | | | | |
| 50 | 800 | 2400 | 125 | 7850 | 1200 | 200 | 0.28 | 2.3 |

**Figure 13.** Recommended shape for steel fiber with rounded wide ends-WESF.

Since the wide ends of WESF are extended perpendicularly inside the matrix, the matrix will produce reaction stresses ($\sigma_{end}$) over the internal side of these ends, and these stresses will be considered as compressive stresses which will work against the applied pull-out force ($F_3$), see Figure 14.

The value of ($F_3$) can be found according to equation (34) as follows:

$$F_3 = \frac{\pi}{4}\left(d^2{}_{end} - d^2\right)f'_c \tag{34}$$

These compressive stresses will add a valuable contribution to the fiber against its pulling out of the matrix. The contribution of these compressive stresses might be estimated as prepared in Table 5, where the fiber-slip force ($F_2$) is the reference. The results of calculations in Table 5 show significant improvements in the performance of fiber/matrix system because of adding the wide ends to the fiber shape. The performance was improved up to 52.65% in case of normal-weight concrete when adding wide ends with diameter ($d_{end}$) greater than the fiber stem diameter ($d$) three times. Whereas, under the same conditions, the performance was improved up to 61.79% in case of sand-lightweight concrete and up to 70.20% in all other types of light-weight concrete, see Figure 15.

## 3.2. Assessment of frictional-slip bond strength performance and the accompanying pressure of surrounding matrix

During the sliding stage, the accompanying pressure of surrounding matrix ($\sigma_x$) will effect on the interface because of the friction between the fiber and the matrix, see
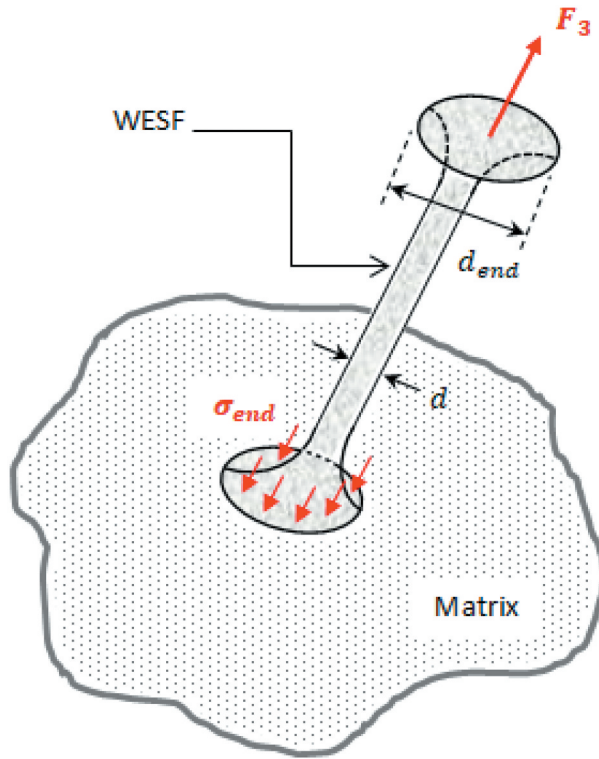
**Figure 14.** Resistance compressive stresses on the rounded wide ends of WESF against applied pull-out force produced by the matrix.

**Table 5.** Estimation of extra pull-out resistance which might be produced as opposite compressive stresses on the internal side of the fiber wide ends.

| Fiber type | $\lambda$ | $f'_c$ (MPa) | $L_{fr}$ (mm) | $d$ (mm) | $d_{end}$ (mm) | $\sigma_P$ (MPa) | $\tau_P$ (MPa) | $F_1$ (N) | $F_2$ (N) | $F_3$ (N) | $(F_1 + F_3/F_2) \times 100$ (%) |
|---|---|---|---|---|---|---|---|---|---|---|---|
| Straight steel fiber-SSF | 1 | 21 | 50 | 0.8 | 0.8 | 2.1 | 2.84 | 1.06 | 178.44 | 0.00 | 0.59 |
| | | | | | 1.6 | | | 4.22 | | 31.67 | 20.11 |
| | | | | | 2.4 | | | 9.50 | | 84.45 | 52.65 |
| | 0.85 | | | | 0.8 | | 2.42 | 1.06 | 152.05 | 0.00 | 0.70 |
| | | | | | 1.6 | | | 4.22 | | 31.67 | 23.60 |
| | | | | | 2.4 | | | 9.50 | | 84.45 | 61.79 |
| | 0.75 | | | | 0.8 | | 2.13 | 1.06 | 133.83 | 0.00 | 0.79 |
| | | | | | 1.6 | | | 4.22 | | 31.67 | 26.82 |
| | | | | | 2.4 | | | 9.50 | | 84.45 | 70.20 |

Figure 7. The pressure of surrounding matrix produces an instant interfacial shear stress ($\tau_s$) in opposite direction of fiber sliding (fiber pull-out direction). This instant interfacial shear stress ($\tau_s$) can be found from the proposed frictional-shear-lag model by satisfying the equilibrium in ($y$) direction as follows:

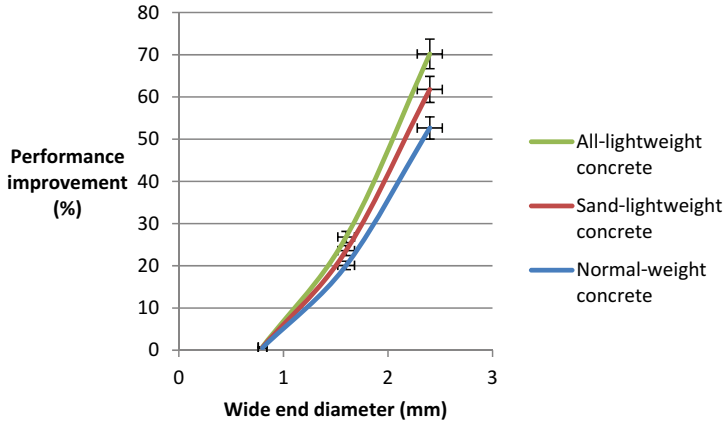$$\tau_s = \frac{P(y)}{\pi d(L_{emb} - u_0)} \tag{35}$$

**Figure 15.** Effect of fiber's rounded wide end diameter on the performance of fiber/matrix system for WESF using different types of concrete matrix, with 5% value error bars.

On the other hand, $(\tau_s)$ can be written in terms of surrounding matrix pressure and friction coefficient, $Fri_{(f.c)}$, at the interface as follows:

$$\tau_s = \sigma_x Fri_{(f.c)} \tag{36}$$

Equating the right side of equations (35) and (36) will give:

$$\sigma_x = \frac{P(y)}{\pi d(L_{emb} - u_0)Fri_{(f.c)}} \tag{37}$$

Substituting, $P(y)$, in equation (37) by its general solution from equation (31) will derive a formula (38), which can be used to find the accompanying pressure of surrounding matrix ($\sigma_x$) during fiber slippage stage as follows:

$$\sigma_x = \frac{\tau_0 \left[ L_{emb} + u_0 \left( \beta \frac{L_{emb}}{d} - 1 \right) \right]}{(L_{emb} - u_0)Fri_{(f.c)}} \tag{38}$$

According to equation (38), if the fiber sliding in the matrix is considered as slip-softening, then ($\beta = 0$) and the formula of accompanying pressure ($\sigma_x$) can be simplified to be as follows:

$$\sigma_x = \frac{\tau_0}{(L_{emb} - u_0)Fri_{(f.c)}} \tag{39}$$

According to equation (39), the distribution of accompanying pressure ($\sigma_x$) along the interface is linear. Therefore, it can be concluded that the fiber-slip mechanism is linear in case of fiber material stiffness is greater than the stiffness of matrix material such as (steel-glass-carbon)-fiber/concrete-matrix, and this result confirms the linear behavior of fiber-slip shown in case (II) Figure 8.

Whereas, if the friction coefficient, $Fri_{(f.c)}$, is found in high ranges, the roughness of fiber surface will damage the matrix surface during the sliding movement; consequently, the collapsed particles will fill the interfacial spaces between the fiber and the matrix, and then the fiber will continue its movement with a smoother sliding. Therefore, it can be

concluded that if the friction of fiber/matrix is high the relationship of pull-out load, $P(y)$, and fiber displacement, $u(y)$, is non-linear and the fiber-slip behavior will be similar to the (III) case in Figure 8 with curvature upward, and this behavior is confirmed according to equation (38) as well, where this behavior can be met in case of steel fiber with high relative roughness.

Moreover, if the matrix stiffness is higher than the fiber stiffness, such as polypropy-lene fiber in concrete matrix, the fiber will stretch under the pull-out load and the roughness of matrix surface will affect the fiber which causes a partial abrasion in the surface of the fiber body. During the progress of fiber sliding and taking the fiber stretching into account, the collapsed pieces of fiber surface are collected between the fiber and the matrix and contribute gradually in resisting the fiber sliding movement. This behavior can be noticed in the (I) case of Figure 8, where the value of shear stress at the interface increases when increasing the applied pull-out load despite decreasing the remain part of embedded length in the matrix until a specific limit, after that the shear stress starts in decreasing because of shortening the remain part of fiber embedded length in the matrix. Therefore, in this case the $(\tau - u)$ relation is non-linear with curvature downward, and this behavior is confirmed according to equation (38) as well.

### 3.3. Pull-Out test results and experimental validation

The results of pull-out tests are important to evaluate the frictional-slip bond character-istics of the four types of fibers (SSF, GF, CF, and Short-SSF) in concrete matrix. Furthermore, the effect of fiber and matrix properties on pull-out behavior can be examined using the experimental results. Moreover, the governing equations, which were derived theoretically, can be validated using the experimental results of this study.

The experimental results of pull-out tests are presented in two categories as follows:

(a) Using embedment length of fiber equal to 50% from its total length.

In this category force-displacement curves of 4 groups of successful samples are drawn as shown in Figure 16. Where, each group was devoted for different type of fiber (SSF, GF, CF, and Short-SSF, and consists of 3 successful samples. Also, observed values of $(S_0, P_{max}, P_0)$ can be seen in Table 6.

(b) Using different ratios of embedment length ranges from 7.5% to 50% from the total length of fiber (L).

In this category force-displacement curves of 2 groups of successful samples are drawn. Where, SSF fiber was used in the first group with different values of embedment length equal to (0.1 L = 5 mm, 0.2 L = 10 mm, 0.3 L = 15 mm, 0.4 L = 20 mm, 0.5 L = 25 mm), and fiber length equal to (L = 50 mm), see Figure 17. Whereas, GF was used in the second group with different values of embedment length equal to (0.075 L = 3 mm, 0.125 L = 5 mm, 0.25 L = 10 mm, 0.5 L = 20 mm), and fiber length equal to (L = 40 mm), see Figure 18.

According to the experimental results of the pull-out test as shown in Figure 16, the frictional sliding part of the force-displacement curve is linear in case of SSF, GF. This result validates the linear behavior which was predicted according to equations (27) and (33). Therefore, it can be concluded that the fiber-slip movement of SSF and GF in normal concrete matrix happens under constant friction and it can be classified in the second case (II) with ($\beta = 0$) as what was shown in Figure 8. Furthermore, the
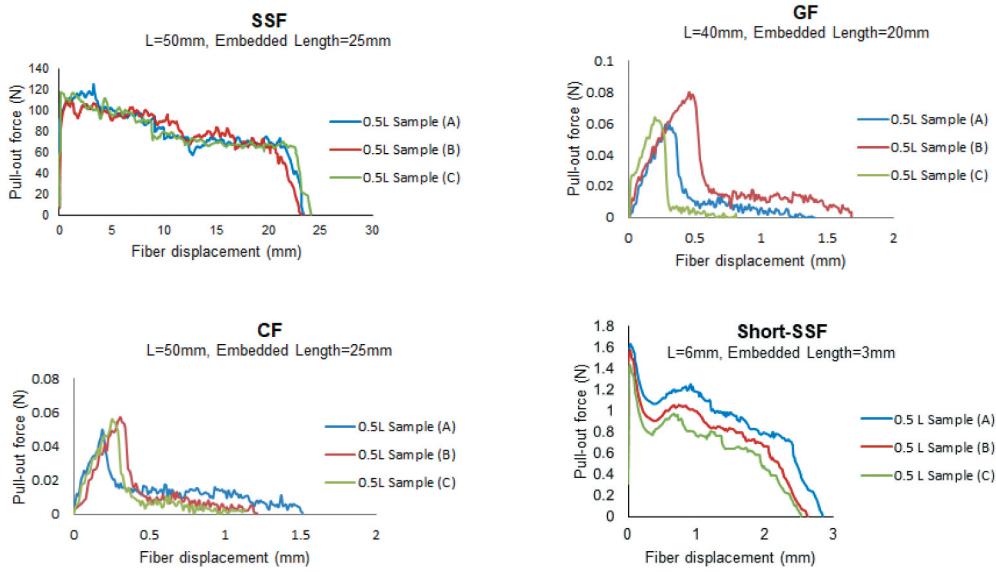
**Figure 16.** Experimental force-displacement curves of single (SSF, GF, CF, and Short-SSF) embedded in normal weight concrete matrix under direct pull-out loading, using same ratio of embedment length equal to 0.5L.

**Table 6.** Observed experimental results (values of $S_0, P_{max}, P_0$).

| Fiber type | $\lambda$ | $f'_c$ (MPa) | $L_{fr}$ (mm) | $d$ (mm) | $L_{fr}/r$ | $S_0$ (mm) | $P_{max}$ (N) | $P_0$ (N) |
|---|---|---|---|---|---|---|---|---|
| Straight steel fiber-SSF | 1 | 21 | 50 | 0.8 | 125 | 0.99 | 125.15 | 103.09 |
| Glass fiber-GF | 1 | 21 | 40 | 0.015 | 5333 | 0.43 | 0.06 | 0.018 |
| Carbon fiber-CF | 1 | 21 | 50 | 0.0075 | 13,333 | 0.39 | 0.05 | 0.01 |
| Short-SSF | 1 | 21 | 6 | 0.16 | 75 | 0.30 | 1.57 | 0.92 |

frictional sliding part of the force-displacement curve is approximately non-linear in case of CF. This result validates the predicted behavior according to equation (31). Therefore, it can be concluded that the fiber-slip movement of CF in a normal concrete matrix happens under non-constant friction and it can be classified in the third case (III) with ($\beta < 0$) as slip-softening behavior with upward curvature, see Figure 8. Finally, in case of Short-SSF, the sliding part in the experimental force-displacement curve looks non-linear with downward curvature; consequently, this behavior matches the first case (I) with ($\beta > 0$), as shown in Figure 8. This experimental result validates the predicted behavior according to equation (31). In case of short fibers such as Short-SSF in concrete matrix, even that fiber is harder than the matrix; the behavior can be classified as slip-hardening (case-I) because of the short embedment length, where shortening the embedment length means that the surrounding matrix will be thin and insufficient to resist the effective shear stresses at the interface, and then the matrix will collapse through strain hardening behavior.

Figure 17 shows that in case of long SSF, it can be noticed that increasing the embedment length of fiber leads to higher pull-out load capacity in a linear behavior as
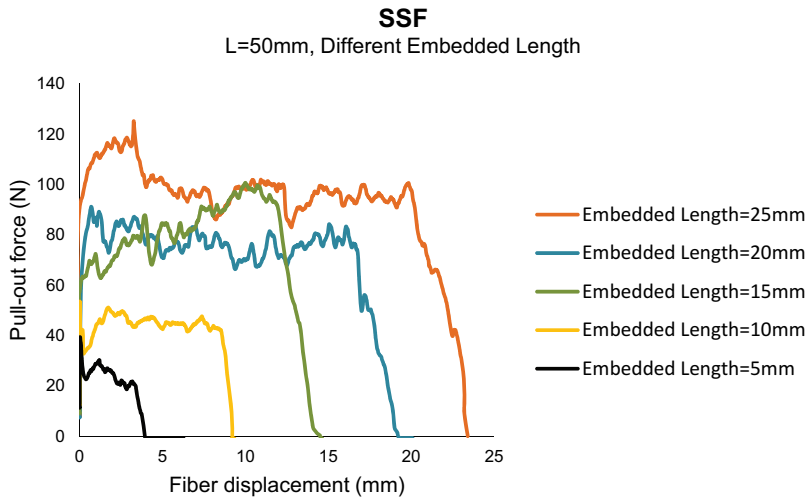
**SSF**
L=50mm, Different Embedded Length



**Figure 17.** Experimental force-displacement curves of single SSF embedded in normal weight concrete matrix under direct pull-out loading, using different values of embedment length.
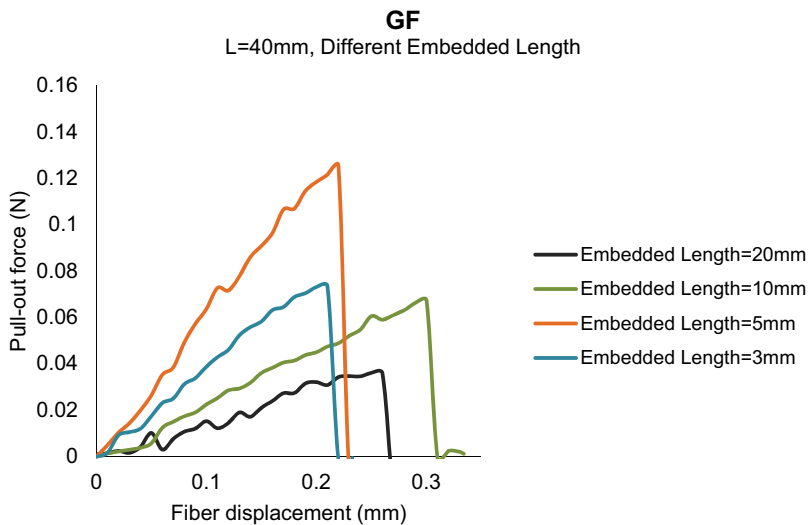
**GF**
L=40mm, Different Embedded Length



**Figure 18.** Experimental force-displacement curves of single GF embedded in normal weight concrete matrix under direct pull-out loading, using different values of embedment length.

shown in Figure 19. This result confirms that the fiber stretching is an important parameter in the pull-out mechanism and it should be taken into account. Also, this result validates and supports as well the assumptions of this study in the theoretical analysis section and governing equations. Furthermore, in case of long GF and CF, it was noticed that the fiber interrupted and cut inside the matrix during debonding stage, and this can be interpreted because of fiber elongation in the cracked part of chemical bond at the interface, in addition to the huge value of fiber aspect ratio ($L_{fr}/r$). Therefore, a sudden cut often happens as shown in Figure 18. This behavior confirms as well the
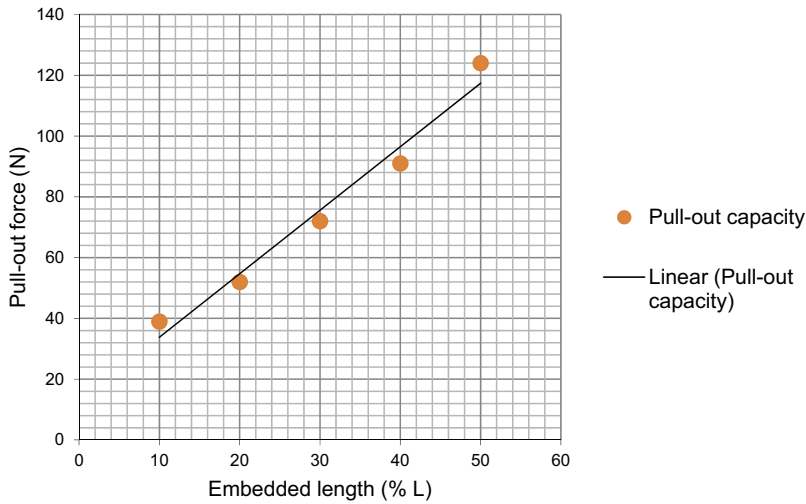
**Figure 19.** Observation of pull-out load changes versus changing the ratio of embedment length in case of SSF.
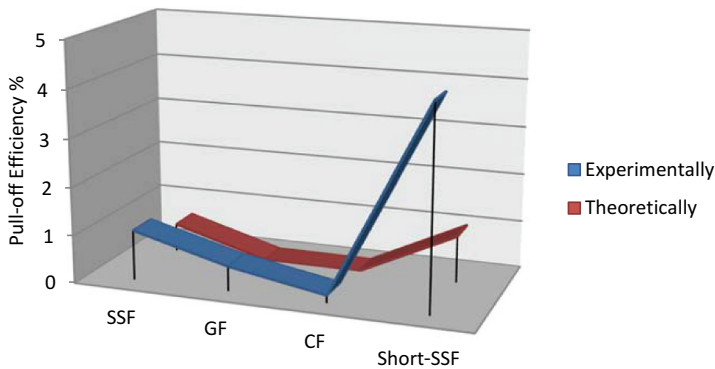


**Figure 20.** Comparison between experimental and theoretical results of pull-off efficiency.

importance of taking the fiber stretching into account in the derivation of governing equations as what was done in this study. While, in case of Sort-SSF, the effect of fiber stretching can be neglected.

Figure 20 shows a comparison between theoretical results and experimental results about the pull-off efficiency for SSF, GF, CF. and Short-SSF. It is clear that the variations are small. Accordingly, it can be concluded that the derived equations are validated by the experimental results.

## 4. Conclusions

This study defined the main parameters which may effect on the fiber slippage behavior in a cementitious-based matrix through theoretical analysis and experimental program.

The theoretical analysis was conducted using a new frictional-shear-lag model. While, in the experimental program many pull-out tests were conducted for selected types of fiber such as (SSF, GF, CF, and Short-SSF). Both theoretical analysis and experimental results showed the importance of fiber-stretch and pull-off bond strength between the fiber and the matrix during fiber-slip movement. The fiber-stretch was included successfully as a main parameter in the derived equations, and the results of these equations were validated by the experimental results. Furthermore, to improve the role of pull-off bond strength, a novel shape of fiber with rounded wide ends-WESF was proposed. This novel-WESF may add good merits in the field of fiber manufacturing.

However, the main conclusions of this study can be summarized in these statements:

- In case of straight steel fiber-SSF, the capacity of pull-out load is increased when increasing the value of embedment length, where it was about 35 MPa and increased to about 121 MPa when increasing the embedded length from 5 mm to 25 mm; and this behavior raises the importance of fiber-stretch to be taken into account.
- In case of glass fiber-GF and CF, increasing the fiber embedment length causes an interruption on the fiber surface during debonding stage, and this leads to a sudden cut in the fiber under lower pull-out load, where theoretically the capacity of glass fiber under direct tension is around 0.26 MPa, but during the pull-out test the fiber cut at pull-out load ranged between (0.036-0.125 MPa). Therefore, it can be concluded that the fiber elongation or fiber-stretch is an important parameter and it should be taken into account.
- In case of short-SSF, the effect of fiber-stretch is small and it can be neglected.
- Increasing the cross-sectional area at the ends of fiber similar to the novel-WESF improves the pull-off bond strength between the fiber and surrounding matrix, where in Novel-WESF the pull-off bond strength improved 52.65% in normal-weight concrete and 70.20% in light-weight concrete, when using the diameter of rounded wide ends 3 times greater than the diameter of fiber stem; and this leads to:
  - (a) Forming an effective transformed region between the full-debonding point and the start point of the frictional sliding stage.
  - (b) Producing additional supporting regions between the fiber and the matrix, which add new restrictions to fix the fiber ends before reaching the full-debonding point, and this activates the elongation property in the fiber (stretching); consequently, the fiber may reach its yield strength (fiber yielding).
  - (c) Improving the capacity of pull-out strength load because of fiber yielding, and this will postpone the start point of fiber slippage.
  - (d) Improving the capacity of frictional-sliding strength due to additional physical friction between the thin edges of wide ends and the matrix.
- The efficiency of pull-off bond strength, in case of normal-weight concrete, is lower than the case of lightweight concretes. While, the higher compressive strength of concrete improves the role of pull-off bond strength.
- The role of pull-off bond strength is more effective in case of steel fiber compared to glass fiber and carbon fiber. Accordingly, the role of pull-off bond strength in case of glass fiber and carbon fiber can be neglected.

- Despite that the results show a higher value of pull-off load capacity in case of long straight steel fiber-SSF compared to the short-SSF, the efficiency of pull-off bond strength in case of short-SSF is higher than the efficiency of pull-off bond strength of the long straight steel fiber-SSF.
- In all types of fiber, the results show that the higher aspect ratio of fiber $(L_{fr}/r)$ effects negatively on the efficiency of pull-off bond strength.
- The novel-WESF showed significant improvements in the performance of the fiber/matrix system because of adding rounded wide ends to the fiber shape. The performance was improved 52.65% in case of normal-weight concrete if the diameter of wide ends is provided three times greater than the fiber stem diameter. Whereas, under the same conditions, the performance was improved 61.79% in case of sand-lightweight concrete and 70.20% in all other types of light-weight concrete.
- Due to different morphology/topology properties of fiber to matrix, the fiber slippage behavior, of (SSF,GF, CF, and Short-SSF) can be classified as follows:
  - (i) Constant friction for SSF and GF/concrete-matrix.
  - (ii) Slip-hardening for short-SSF/concrete-matrix.
  - (iii) Slip-softening for CF/concrete-matrix.

## Acknowledgment

## Disclosure statement

No potential conflict of interest was reported by the author(s).

## ORCID

Amjad Khabaz http://orcid.org/0000-0001-6591-3802

## Data Availability

The raw/processed data required to reproduce these findings cannot be shared at this time due to technical or time limitations.

## References

[1] Pi Z, Xiao H, Li H. Influence of interfacial microstructure on pullout behavior and failure mechanism of steel fibers embedded in cement-based materials. Constr Build Mater. 2021;304:124688.
[2] Lee SK, Oh T, Chun B, et al. Surface refinement of steel fiber using nanosilica and silver and its effect on static and dynamic pullout resistance of reactive powder concrete. J Build Eng. 2022;51:104269.
[3] Aragão S, Júnior A, Parvin A. Reinforcement of new and existing reinforced concrete beams with fiber-reinforced polymer bars and sheets – a numerical analysis. Structures. 2022;40:513–523.

[4] Chalioris CE, Karayannis CG. Effectiveness of the use of steel fibres on the torsional behaviour of flanged concrete beams. Cem Concr Compos. 2009;31(5):331–341.

[5] Kytinou VK, Chalioris CE, Karayannis CG, et al. Effect of Steel Fibers on the Hysteretic Performance of Concrete Beams with Steel Reinforcement—Tests and Analysis. Materials. 2020;13(13):2923.

[6] Chalioris CE, Kosmidou P-M, Karayannis CG. Cyclic Response of Steel Fiber Reinforced Concrete Slender Beams: an Experimental Study. Materials. 2019;12(9):1398.

[7] Golewski GL. Physical characteristics of concrete, essential in design of fracture-resistant, dynamically loaded reinforced concrete structures. Mat Design Process Comm. 2019;1(5): e82.

[8] Golewski GL, Szostak B. Application of the C-S-H Phase Nucleating Agents to Improve the Performance of Sustainable Concrete Composites Containing Fly Ash for Use in the Precast Concrete Industry. Materials. 2021;14(21):6514.

[9] Bilotta A, Lignola GB. Effect of fiber-to-matrix bond on the performance of inorganic matrix composites. Compos Struct. 2021;265:113655.

[10] Cox HL. The elasticity and strength of paper and other fibrous materials. Br J Appl Phys. 1952;3(3):72–79.

[11] Khabaz A. Theoretical analysis and numerical simulation of development length of straight steel fiber in cementitious materials. Compos Interfaces. 2017;24(5):447–467.

[12] Landis CM, McMeeking RM. A shear-lag model for a broken fiber embedded in a composite with a ductile matrix. Compos Sci Technol. 1999;59(3):447–457.

[13] Curtin WA. Theory of mechanical properties of ceramic matrix composites. J Am Ceram Soc. 1991;74(11):37–45.

[14] Lawrence PJ. Some theoretical considerations of fiber pull-out from an elastic matrix. J Mater Sci. 1972;7(1):1–6.

[15] Freund LB. The axial force needed to slide a circular fiber along a hole in an elastic material and implications for fiber pull-out. Euro J Mech, A/solids. 1992;11(1):1–19.

[16] Fuller JE, Butler EP, Carter WC. Determination of fiber matrix interfacial properties of importance to ceramic composite toughening. In: Shah SP, Fuller, JE, Butler, EP, Carter, WC. editor. Proc., NA to Advanced Res. Workshop on Toughening Mechanisms in Quasi-Brittle Mat. Dordrecht, Netherlands: Kluwer Academic Publishers; 1991. pp. 385–404.

[17] Shah SP, Ouyang C. Mechanical behavior of fiber-reinforced cement-based composites. J Am Ceram Soc. 1991;74(11):2727–2738, 2947-53. 10.1111/j.1151-2916.1991.tb06836.x.

[18] Bazant ZP, Gambarova PG. Rough cracks in reinforced concrete. J Struct Div, ASCE. 1980;106(4):819–842.

[19] Divakar MP, Fafitis A, Shah SP. Constitutive model for shear transfer in cracked concrete. J Struct Div, ASCE. 1987;113(5):1046–1062.

[20] Feenstra PH, de Borst R, Rots JG. Numerical study on crack dilatancy. J Engrg Mech, ASCE. 1991;117(4):733–769.

[21] Zdeněk PB, Rodrigue D. Size Effect in Fiber or Bar Pullout with Interface Softening Slip. J Eng Mech ASCE. 1994;120(9):1945–1962.

[22] Gao BYC, Mai YW, Cotterell B. Fracture of fiber-reinforced materials. Zamp. 1988;39:550–572.

[23] Khabaz A. Assessment of frictional-bond strength at the interface of single SSF in cementitious composite and prediction of accompanying pressure of surrounding matrix. Compos Interfaces. 2022;29(7):765–793.

[24] Gopalaratnam VS, Shas SP. Tensile fracture of steel fibre reinforced concrete. ASCE J Eng Mech. 1987;113(5):635–652.

[25] Khabaz A. Prediction of (Steel-Glass) Fiber/Concrete Interfacial Friction Properties in FRC Composites Using Calibration Method and Evaluation of Fiber Diameter Role. ASCE J Mater Civ Eng. 2022;34(2):04021438.

[26] Khabaz A. Experimental and Numerical Investigation of Single Fiber Pull-Out Tests of Steel Macro-Fiber and Glass Micro-Fiber in a Cementitious Matrix. ASTM J Test Eval. 2022;50 (1):401–418.

[27] Wang Y, Li VC, Backer S. Modeling of fiber pull-out from a cement matrix. Int J Cement Compos Lightweight Con. 1988;10(3):143–149.

[28] Redon C, Li VC, Wu C, et al. Measuring and Modifying Interface Properties of PVA Fibers in ECC Matrix. J Mater Civ Eng. 2001;13(6):399–406. 10.1061/(ASCE)0899-1561(2001) 13:6(399)

[29] Marshall DB. Analysis of fiber debonding and sliding experiments in brittle matrix composites. Acta Metall Mater. 1992;40(3):427–441.

[30] Khabaz A. Determination of Friction Coefficient Between Straight Steel Fiber and the Concrete Fri ($($_{(ssf.C)}$)$). Adv Mater. 2015;4(2):20–29.

[31] Khabaz A. Determination of Friction Coefficient between Glass Fiber and the Concrete Fri$_{(GF.C)}$. Int J Mater Sci Appl. 2014;3(6):321–324.

[32] Yoo DY, Kim S, Kim JJ, et al. An experimental study on pullout and tensile behavior of ultra-high-performance concrete reinforced with various steel fibers. Construct Build Mater. 2019;206:46–61.

[33] Shannag MJ, Brincker R, Hansen W. Pullout behavior of steel fibers from cement-based composites. Cem Concr Res. 1997;27(6):925–936.

[34] Chun B, Yoo DY, Banthia N. Achieving slip-hardening behavior of sanded straight steel fibers in ultra-high-performance concrete. Cement Concr Compos. 2020;113:103669.

[35] Lee Y, Kang ST, Kim JK. Pullout behavior of inclined steel fiber in an ultra-high strength cementitious matrix. Construct Build Mater. 2010;24(10):2030–2041.

[36] Kim JJ, Jang YS, Yoo DY. Tensile properties of ultra-high-performance concrete improved by novel curvilinear steel fibers. J Mater Res Tech. 2020;9(4):7570–7582.

[37] Yoo DY, Choi HJ, Kim S. Bond-Slip response of novel half-hooked steel fibers in ultra-high-performance concrete. Constr Build Mater. 2019;224:743–761.

[38] Khabaz A. Impact of fiber shape on mechanical behavior of steel fiber in fiber reinforced concrete FRC. World J Eng Phys Sci. 2015;3(1):001–006.

[39] Khabaz A. Monitoring of impact of hooked ends on mechanical behavior of steel fiber in concrete. Constr Build Mater. 2016;113:857–863.

[40] Khabaz A. Performance evaluation of corrugated steel fiber in cementitious matrix. Constr Build Mater. 2016;128:373–383.

[41] Li Y, Liu YL, Peng XH, et al. Pull-Out simulations on interfacial properties of carbon nanotube-reinforced polymer nanocomposites. Comput Mater Sci. 2011;50:1854–1860.

[42] Şahmaran M, Christianto HA, Yaman I. The effect of chemical admixtures and mineral additives on the properties of self-compacting mortars. Cem Concr Compos. 2006;28 (5):432–440.

[43] Mpalaskas AC, Vasilakos I, Matikas TE, et al. Monitoring of the fracture mechanisms induced by pull-out and compression in concrete. Eng Fract Mech. 2014;128:219–230.

[44] Khabaz A. Dynamical analysis of non-metallic (glass, carbon) fiber reinforced concrete under the influence of vibration. Int J Comp Mater. 2013;3(6):174–180.

[45] Deng F, Ding X, Chi Y, et al. The pull-out behavior of straight and hooked-end steel fiber from hybrid fiber reinforced cementitious composite: experimental study and analytical modelling. Compos Struct. 2018;206:693–712.

[46] Zhan Y, Meschke G. Analytical model for the pullout behavior of straight and hooked-end steel fibers. J Eng Mech. 2014;140(12):04014091.

[47] Yang EH, Wang S, Yang Y, et al. Fiber-Bridging Constitutive Law of Engineered Cementitious Composites. J Adv Concr Technol. 2008;6(1):181–193.

[48] Li VC. Engineered Cementitious Composites (ECC) Bendable Concrete for Sustainable and Resilient Infrastructure. Springer; 2019.

[49] Bao G, Song Y. Crack bridging models for fiber composites with degraded interfaces. J Mech Phys Solids. 1993;41(9):1425–1444.